ChemPubSoc Europe

DOI: 10.1002/chem.201500086

CHEMISTRY A European Journal Full Paper

Self-Assembly

Designed Intercalators for Modification of DNA Origami Surface Properties

Josipa Brglez, Pavel Nikolov, Alessandro Angelin, and Christof M. Niemeyer*[a]

Abstract: The modification of the backbone properties of DNA origami nanostructures through noncovalent interactions with designed intercalators, based on acridine derivatized with side chains containing esterified fatty acids or oligo(ethylene glycol) residues is reported. Spectroscopic analyses indicate that these intercalators bind to DNA origami structures. Atomic force microscopy studies reveal that intercalator binding does not affect the structural intactness but leads to altered surface properties of the highly negatively charged nanostructures, as demonstrated by their interaction with solid mica or graphite supports. Moreover, the noncovalent interaction between the intercalators and the origami structures leads to alteration in cellular uptake, as shown by confocal microscopy studies using two different eukaryotic cell lines. Hence, the intercalator approach offers a potential means for tailoring the surface properties of DNA nanostructures.

Introduction

The so-called "scaffolded DNA origami" technique[1] employs a long single-stranded DNA (ssDNA) scaffold which is folded into arbitrary shape by aid of short synthetic "staple strand" oligonucleotides. Arguably, this technique has revolutionized our capabilities to access an unlimited variety of finite DNA nanostructures,[2,3] which are currently being exploited, in particular, as molecular pegboards for the precise arrangement of molecular and colloidal components. The latter can encompass a diverse spectrum of components ranging from small molecules and proteins over nanoparticles to nucleic acid-based probes.[4–9] In spite of the variability of the origami-tethered ligands, the nature of the origami scaffold is largely restricted to negatively charged (deoxy)ribonucleic acids, and thus particular aspects of applications of ligand-decorated origami constructs have to be adapted to the highly charged nature of the nucleic acid scaffold.

We here report on the modification of the backbone properties of DNA nanostructures through noncovalent interactions with designed intercalators derivatized with side chains containing either esterified fatty acids or oligo(ethylene glycol) residues. Intercalators are small molecule probes which can insert between the stacked planar bases of double-stranded DNA (dsDNA).[10] Owing to the fact that they can be used for the control of DNA structure in bioanalytical and biomedical settings,[11] intercalators are widely applied in analytical and medicinal chemistry,[12] and mechanistic insights into their mode of action are steadily increased by modern biophysical techniques, such as magnetic tweezers[13] or time-lapse AFM imaging.[14] In the context of structural DNA nanotechnology, intercalators have been used as fluorophore units in dye arrays on a 3D DNA-tetrahedron nanostructure,[15] or as cargo of origami-based drug delivery vehicles for circumvention of drug resistance.[16,17] Recently, Ke et al. employed a specific DNA origami design strategy, the underwinding of double helices, to increase the affinity for intercalators, and they used this enhanced affinity for binding a PEG-tris-acridine compound.[18] While this work represents an elegant demonstration that noncovalent interactions can be tuned by design of DNA nanostructures, this approach is still in its infancy and the properties of the resulting supramolecular assemblies have not yet been explored. Moreover, it is yet unknown whether and how intercalators with different chemical properties, for example, hydrophilicity versus lipophilicity, can be used to modify the surface properties of DNA nanostructures.

Results and Discussion

We reasoned that the covalent tethering of an intercalating acridine unit with different side chains should lead to novel noncovalent modifiers for DNA origami structures. To investigate this hypothesis, we synthesized two acridine derivatives (**1**, **2** in Scheme 1) which contained a hexaethyleneglycol- or bis-(hexadecyloxy)propyl-hexanoate side chain, respectively, from the common precursor 9-chloroacridine (**3**; Scheme 1).

Both derivatives, hydrophilic ethyleneglycol-acridine (**1**), in the following denoted as EG-Acr, and lipophilic bis-palmitoylglycerol-acridine (**2**), denoted as L-Acr, were obtained as pure compounds in satisfactory yields of 69 and 27%, respectively.

[a] J. Brglez, Dr. P. Nikolov, A. Angelin, Prof. Dr. C. M. Niemeyer
Karlsruhe Institute of Technology (KIT)
Institute for Biological Interfaces (IBG 1), Hermann-von-Helmholtz-Platz
76344 Eggenstein-Leopoldshafen (Germany)
E-mail: niemeyer@kit.edu

Supporting information for this article is available on the WWW under http://dx.doi.org/10.1002/chem.201500086.

© 2015 Wiley-VCH Verlag GmbH & Co. KGaA, Weinheim

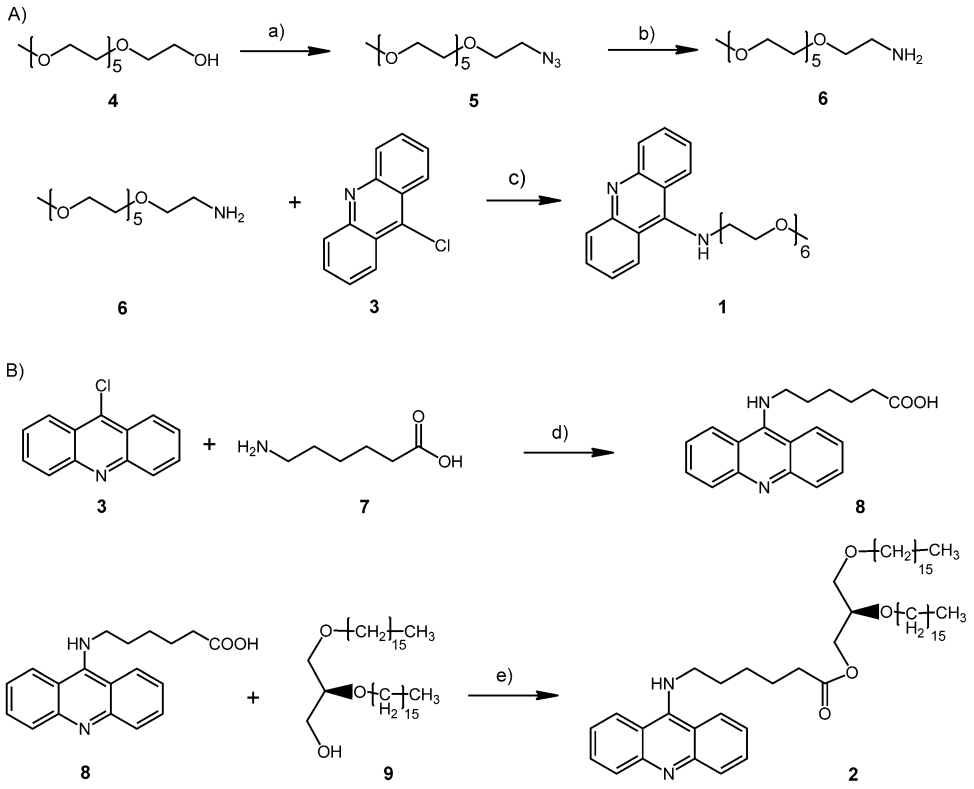

Scheme 1. Synthetic route to acridine-based origami ligands EG-Acr (**1**) and L-Acr (**2**); a) MsCl, TEA in dry DCM, 0–4 °C, 24 h; NaN_3, DMF, 70 °C, 3 h; b) PPh_3 in dry THF, 0 °C, 10 h, then H_2O, 10 h; c) **6** + **3**, THF, 60 °C, 12 h; d) phenol, 100 °C, 80 min, then **7**, 100 °C, 2 h; e) **8** + **9**, DCC/DMAP, DMF, RT, 3 h.

The detailed description of experimental procedures and characterization of compounds is given in the Supporting Information.

In a first set of experiments, binding capabilities of EG-Acr and L-Acr for regular dsDNA was investigated through spectroscopic equilibrium-binding titration analyses to determine affinity constants (Figure 1). To this end, EG-Acr and L-Acr ligand solutions were prepared in buffer and in DMSO, respectively, and progressive absorbance changes were monitored for free ligands and ligand–DNA complexes, upon addition of increasing amounts of dsDNA (Figure 1 A).

Indeed, addition of dsDNA led to decrease in absorbance and the observed changes were converted into binding isotherms (Figure 1 B) using a neighbor-exclusion model, allowing the estimation of the dissociation constants for the ligands interacting with dsDNA.[19] Dissociation constants were determined as 59 and 44 μM for EG-Acr and L-Acr, respectively, which are close to data reported for structurally similar compounds, 9-aminoacridine[20] or methylene blue.[21] Since typical binding constants for intercalation complexes between similar aromatic compounds and dsDNA range from 10^4 to 10^6 M^{-1},[22] the data measured for L-Acr and EG-Acr, provided initial evidence for intercalation of the acridine unit within the double helix. Continuous variation binding analysis (Job's plot) was performed to determine the stoichiometry of the binding (Figure 1 C). While a single maximum was observed in the Job's plot of EG-Acr, the curve obtained for L-Acr revealed multiple binding modes suggesting at least two different types of DNA–intercalator complexes. Indeed, the high lipophilicity of L-Acr led to low solubility in aqueous media and dynamic light scattering (DLS) measurements indicated the formation of micelles at concentrations greater than approximately 0.4 μM (Figure S1 in the Supporting Information). Hence, we reason that the multiple binding types are associated with formation of higher-order structures. Although limited amounts of material precluded the determination of binding constants of EG-Acr and L-Acr for DNA origami nanostructures, fluorometric analysis provided clear evidence, that both ligands indeed bind the origami nanostructure (Figure S2 in the Supporting Information).

We then investigated whether binding of EG-Acr or L-Acr leads to changes in the morphology and affects adsorption behavior of DNA origami structures. To this end, a rectangular DNA origami structure of approximately 91×54 nm^2 was assembled using the circular single-stranded 5438 nucleotide plasmid ss109Z5.[23] AFM images of these origami plates adsorbed onto Mg^{2+}-activated mica revealed that the nanostructures were formed in almost quantitative yields (left image in Figure 2 A). Treatment of the origami structures with lipophilic L-Acr or hydrophilic EG-Acr affected their capability to adsorb to the hydrophilic mica surface (middle and right image in Figure 2 A, respectively). Lowered amounts of EG-Acr–, and in particular of L-Acr–origami, were adsorbed to mica, thereby providing evidence for altered surface properties of the noncovalently modified DNA nanostructures. Statistical analysis of the AFM images indicated that lateral (*x*,*y*) dimensions of the origami were not significantly altered upon binding of L- or EG-Acr ligands (Figure 2 B).

However, height analysis revealed significant differences between unmodified und intercalator-modified origami structures. In particular, we determined a typical average height of planar 2D origami of approximately 1 nm, which was lower than the theoretical value 2 nm, due to typical flattening of biomolecules by the AFM tip.[24] The height of unmodified origami was increased by a factor of 2.5 or 3 in the case of EG- and L-Acr binding, respectively. Since model calculations indicate a length of about 2.3 and 2.8 nm for EG- and L-Acr, respectively (Figure S3 in the Supporting Information), the AFM data suggest dense arrangements of the Acr-ligands protruding from both sides of the origami.

© 2015 Wiley-VCH Verlag GmbH & Co. KGaA, Weinheim

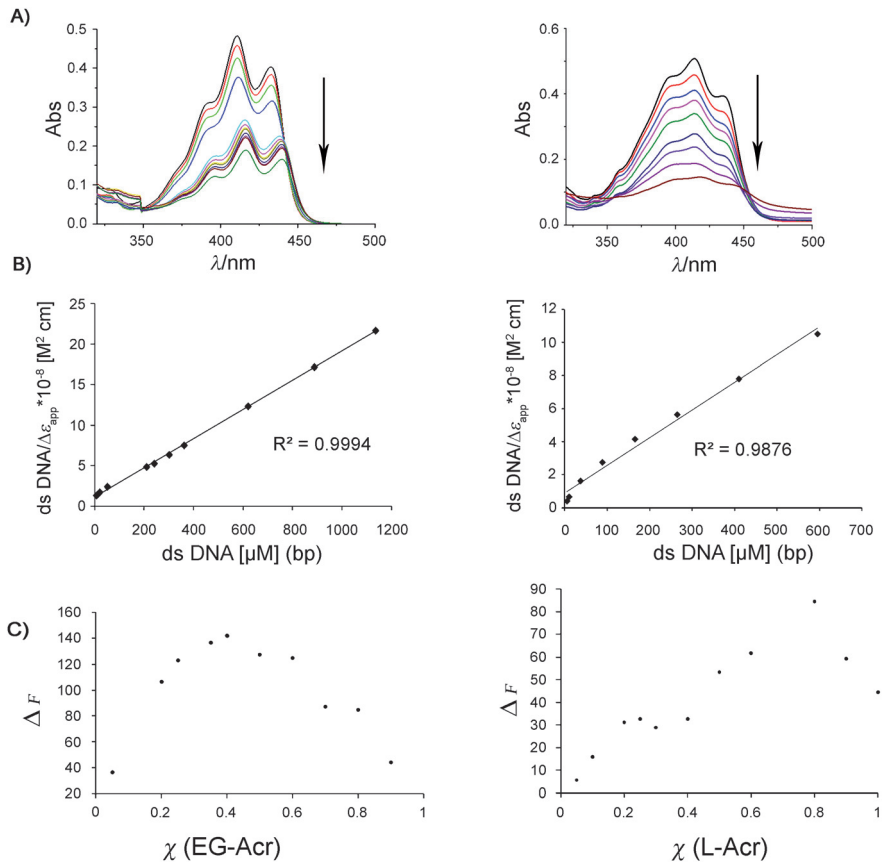

Figure 1. Spectroscopic characterization of EG-Acr (**1**; left panel) and L-Acr (**2**; right panel). A) Representative spectra of the titration of acridine ligands with increasing amounts of dsDNA led to progressive decrease in absorbance. B) The observed changes in absorbance (dsDNA/$\Delta\varepsilon_{app}\times$[M^{2}cm]) were plotted against dsDNA concentration to generate binding isotherms for determination of affinity constants. C) Continuous variation binding analysis (Job's plot), used to determine binding stoichiometry, indicates a single maximum for EG-Acr (left panel), while the curve obtained for L-Acr revealed multiple binding modes, suggesting at least two different types of DNA–intercalator complexes (right panel).

To follow up on the hypothesis that EG- and L-Acr binding affects the origami's surface properties and thus its adsorption behavior, we also investigated physisorption to the very hydrophobic substrate HOPG (highly-oriented pyrolytic graphite), which is often used for scanning-tunneling microscopy studies on the self-assembly of lipophilic small molecules.[25] Unmodified origami adsorbed to HOPG only in the presence of low concentrations of detergents (Tween 20, 0.05% v/v) and the adsorption to HOPG led to severe damage of the nanostructures (left image, in Figure 2C). We hypothesize that the disruption of the folded structure results from favored van der Waals and stacking interactions between the DNA nucleobases and the HOPG surface which induce dehybridization of double helices and an unfolding of the nanostructures. While no adsorption could be achieved for EG-Acr-modified origami, the L-Acr-modified origami adsorbed to a significantly larger extent on the HOPG (Figure 2C, middle). In this case, more intact origami structures were observed, suggesting that intercalation of L-Acr increased the binding capability and also stabilized the folding of the nanostructures. Interestingly, stabilization of the origami structure was also observed when streptavidin (STV) molecules were bound to one side of the origami using biotinylated staple strands (right image, in Figure 2C). To explain this phenomenon, we reason that the STV proteins reduce the overall negative charge of the DNA origami, thereby stabilizing the integrity of the structures. It is evident, however, that more detailed investigations are necessary to unravel mechanistic details of DNA nanostructure–surface adsorption processes.

To further explore how intercalation affects the origami's surface properties, we studied their uptake by eukaryotic cells. Two cell lines, HeLa and L929, were used in these experiments. In addition to unmodified, L-Acr- or EG-Acr-modified origami structures, an origami construct bearing ten cholesterol ligands was used as control. All origami structures were labeled with nine Cy5 molecules to enable their fluorescent detection by confocal laser scanning microscopy (CLSM). In agreement with earlier studies,[16,17,26,27] DNA origami structures were stable in cell culture medium for at least 24 h (Figure S4 in the Supporting Information). The presence of the various origami samples (290 pM final concentration) in culture medium had no harmful effects on the cells (Figure S5 in the Supporting Information). In particular, the viability of L929 cells exposed to DNA origami was not changed during a period of four days. Moreover, cells proliferated and their viability was not affected by the DNA nanostructures. Further analysis of cells was conducted by CLSM microscopy (Figure 3).

The results showed clear evidence that loading of origami with both L-Acr or EG-Acr led to an increased cell uptake, as compared to unmodified origami. In fact, intercalation-based, noncovalent modification was as effective as covalent modification with cholesterol (Figure 3B). Notably, the increased uptake of L-Acr- or EG-Acr-modified origami was consistently observed for both L929 and HeLa cell lines (Figure 3B and C, respectively, see also Figure S6 in the Supporting Information). The *z*-stack reconstruction of 3D confocal images (Figure 3D and Figure S7 in the Supporting Information) provided clear evidence that origami was internalized by the cells. Furthermore, the combined MitoTracker Green staining showed a pattern of partial co-localization of DNA origami with the mitochondrial compartment, confirming the internalization of both unmodified and ligand-modified nanostructures (Figure S6).

© 2015 Wiley-VCH Verlag GmbH & Co. KGaA, Weinheim

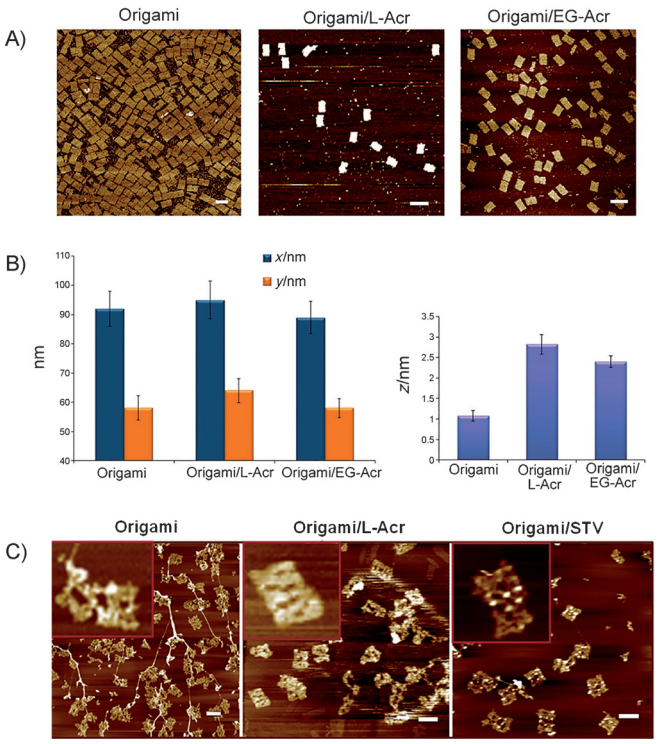

Figure 2. AFM analyses of DNA origami structures. A) Representative AFM images of unmodified DNA origami (left), L-Acr- (middle) or EG-Acr-modified origami (right) adsorbed to hydrophilic mica substrates; scale bar: 100 nm. Note that unmodified origami binds to the surface in high density, while low and medium density surface coverages are observable for L-Acr- or EG-Acr-modified origami. B) Statistical analysis of lateral dimensions and height of the origami structures ($N \geq 100$). C) Adsorption of unmodified DNA origami (left), L-Acr- (middle) and STV-modified (right) origami an hydrophobic HOPG substrates. Note that L-Acr or STV modification appears to stabilize the integrity of the DNA nanostructures.

Conclusion

In conclusion, we here demonstrate that designed intercalators can be used for noncovalent modification of origami structures. In particular, we found that acridine derivatives equipped with esterified lipid acids or ethyleneglycol side chains bind to DNA origami structures and induce significantly changed surface properties of the nanostructures, as documented by their interaction with solid supports (mica, HOPG) and cellular membranes. Despite this clear experimental evidence, the detailed mechanistic modes of action remain presently unclear and further studies are required to unravel details of DNA nanostructure–surface interaction. Nonetheless, the results of this study suggest that the intercalator approach has a high potential for tailoring surface properties of DNA nanostructures in a noncovalent and thus transient fashion. We therefore anticipate that this strategy might prove useful for further exploitation of structural DNA nanotechnology.

Experimental Section

Synthesis of methoxyhexaethylene glycol amine (6)

Hexaethylenamine **6** was synthesized according to established procedures.[28,29] In brief, a solution of anhydrous HEG **4** (500 mg, 1.68 mmol) and TEA (0.28 mL, 2 mmol) in dry CH_2Cl_2 (30 cm^3) was cooled to 0 °C. A solution of methanesulfonyl chloride (0.15 mL, 2.02 mmol) in CH_2Cl_2 (3 mL) was slowly added under stirring and the reaction was then maintained at 4 °C for 24 h. The solvent was evaporated and the crude material was purified by silica gel column chromatography using 0–15% gradient of MeOH in DCM to give monomesylate (89%). The product (TLC in DCM/MeOH 9:1, $R_f = 0.42$) was used without further purification. Sodium azide (182 mg, 2.8 mmol) was added to a solution of monomesylate (559 mg, 1.4 mmol) in dry DMF (2 mL). The mixture was heated at 70 °C for 2.5 h and then allowed to cool to room temperature. DMF (3 mL) was added to improve azide solubility. The reaction mixture was co-evaporated with toluene at 50 °C, and the residue was purified by chromatography using a 0–15% gradient of MeOH in DCM giving 417 mg (92%) of methoxyhexaethylene glycol azide **5**. ESI-MS: calcd for $C_{13}H_{27}N_3O_6$ $[M+H]^+$ 322.19; found $[M+H]^+$ 322, $[M+Na]^+$ 344.13. A solution of **5** (200 mg, 0.62 mmol) in dry THF (2 mL) was cooled to 0 °C. Triphenyl phosphine was added (184 mg, 0.69 mmol) and the mixture was allowed to reach room temperature. The reaction was monitored by TLC (*i*PrOH/aqueous NH_3 (0.05%)/H_2O 6:3:1). After 10 h water was added (30 μL) to hydrolyze the intermediate phosphorus adduct and the mixture was stirred, overnight (< 10 h). The reaction mixture was diluted with water and washed with toluene. Evaporation of the aqueous layer yielded 154 mg (84%) of methoxyhexaethylene glycolamine compound **6**, which was used in the next step without further purification. ESI-MS: calcd for $C_{13}H_{29}NO_6$ $[M+H]^+$ 296.2; found $[M+H]^+$ 296.2. ^{1}H NMR ([D]CDCl$_3$): $\delta = 3.36$ (s, 3H), 2.87 (t, 2H), 3.51–3.55 (m, 4H), 3.64 ppm (s, 18H); ^{13}C NMR: $\delta = 41.6$, 58.9, 70.2, 70.5, 71.8, 72.8 ppm.

Synthesis of ethyleneglycol-acridine (EG-Acr; 1)

The 9-chloroacridine **3** (Sigma–Aldrich, 226 mg, 1.05 mmol) was dissolved in dry THF (2 mL) under Ar. Compound **6** (155 mg; 0.52 mmol) was dissolved in dry THF (3 mL) and then mixed with the solution of **3**. After stirring overnight at 60 °C, the solvent was evaporated and the product was purified by silica gel chromatography using 2–18% gradient of MeOH in DCM to obtain **1** in 69% yield. ESI-MS: calcd for $C_{26}H_{36}N_2O_6$ $[M+H]^+$ 473.26; found $[M+H]^+$ 473.33. ^{1}H NMR ([D]CDCl$_3$): $\delta = 3.36$ (s, 3H), 3.52 (m, 3H), 3.59–3.62 (m, 15H), 3.69 (t, 2H) 3.8 (t, 2H), 7.25–7.29 (d, 2H), 7.55 (t, 2H), 8.18 (d, 2H), 8.47 (d, 2H), 9.4 (s, 1H), 14.2 ppm (s, 1H); ^{13}C NMR: $\delta = 48.1$, 58.6, 70.1, 71.5, 119.1, 122.8, 132.6, 157.05 ppm.

Synthesis of 6-(acridin-9-ylamino)hexanoic acid (8)

The 6-(acridin-9-ylamino)hexanoic acid (**8**) was synthesized according to published procedures.[30] In brief, a mixture of 9-chloroacridine **3** (1 g, 4.68 mmol) and phenol (5 g, 0.05 mol) were stirred at 100 °C for 80 min and then 6-aminocapronic acid (**7**; 676 mg, 5.15 mmol) was added. The reaction mixture was incubated at 100 °C for 2 h. After cooling to RT, the solvent was removed in vacuo and the crude product (1.5 g) was purified by silica gel flash chromatography (Biotage, 50 g column) using 4–20% gradient of MeOH (0.05% HOAc) in DCM in 25 column volumes (CV) to obtain the final product **8** in 95% yield. ESI-MS calcd for $C_{19}H_{20}N_2O_2$ $[M+H]^+$ 309.15; found $[M+H]^+$ 309.2; $[M-H]^-$ 307.2. ^{1}H NMR

© 2015 Wiley-VCH Verlag GmbH & Co. KGaA, Weinheim

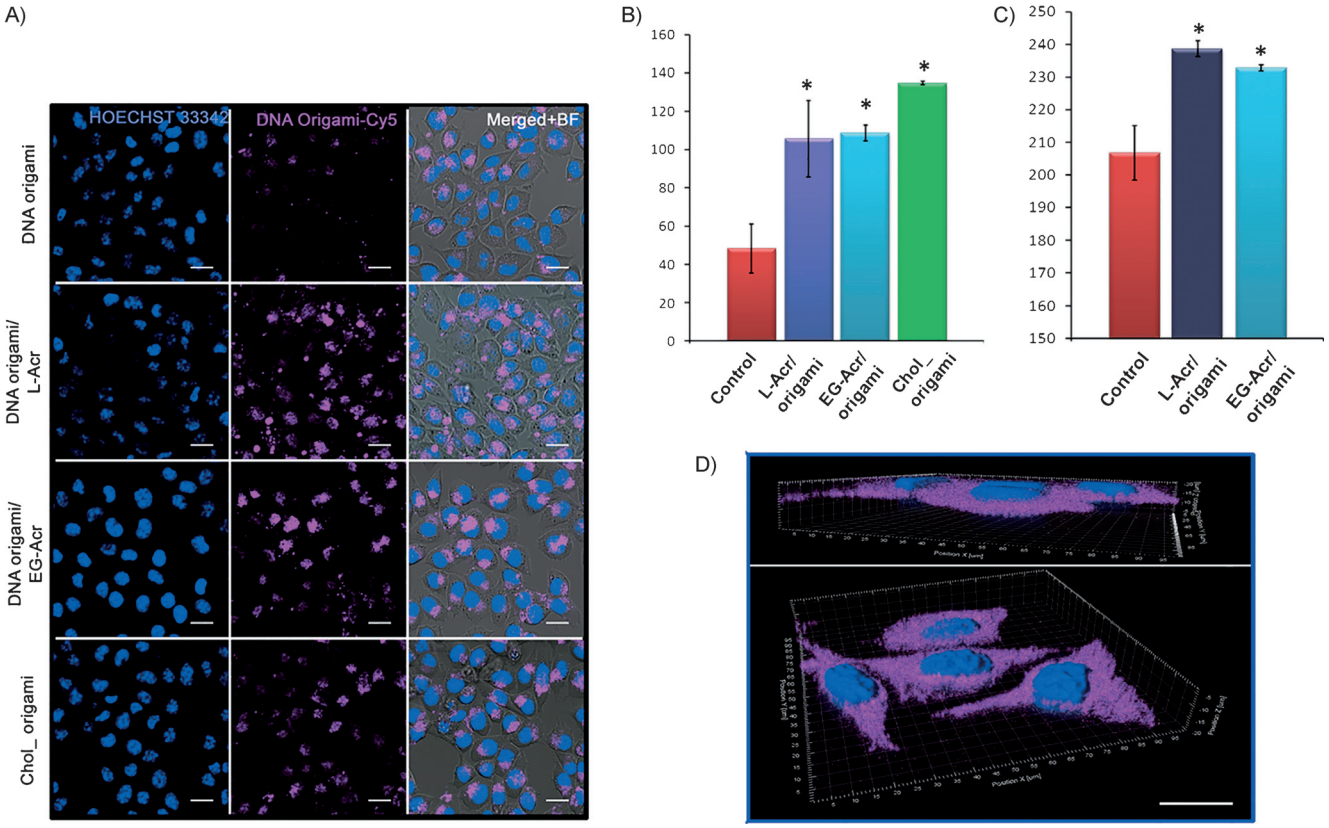

Figure 3. Confocal laser scanning microscopy (CLSM) analysis of DNA origami uptake by L929 fibroblasts and HeLa cells. A) CLSM images of L929 cells treated with unmodified DNA origami, L-Acr- or EG-Acr-modified origami. An origami construct bearing ten cholesterol ligands was used as control (bottom row of images). All origami structures contained nine Cy5 molecules to enable fluorescent detection. Cell nuclei were counterstained with Hoechst 33342 (scale bars: 20 μm; conditions: 3×10^4 cells mL^{-1}, 2.5 nM DNA origami, one ligand per bp, 6 h incubation). B) Statistical analysis of fluorescence signals of Cy5-labeled origami. Values were calculated as mean ± SD from at least two independent measurements. Statistical significance was evaluated by one-way ANOVA, followed by Dunnett's multiple comparison test (*$p<0.0001$). C) Statistical analysis of CLSM images obtained for uptake experiments with HeLa cells (for original data, see Figure S5 in the Supporting Information). D) The *z*-stack projection of CLSM images, obtained from HeLa cells treated with L-Acr-loaded DNA origami.

([D_6]DMSO): $\delta=1.4$ (m, 2H), 1.55 (m, 2H), 2.22 (t, 2H), 4.05 (t, 2H), 7.5 (t, 2H), 7.95 (m, 4H), 8.58 ppm (d, 2H); ^{13}C NMR: $\delta=24.12$, 28.81, 33.54, 48.77, 119.25, 123.03, 125.88, 134.29, 156.68, 174.41, 214.22, 228.37 ppm.

Synthesis of bis-palmitoyl-glycerol-acridine (L-Acr; 2)

Preparation of L-Acr (**2**) was adopted from a known procedure.[31] To a stirred solution of carboxylic acid **8** (22 mg, 0.065 mmol) in 1 mL anhydrous DMF, DMAP (0.85 mg, 0.017 mmol; 10% mol) and 1,2-di-*O*-hexadecly-sn-glycerol **9** (77 mg, 0.14 mmol, Bachem) were subsequently added. The reaction mixture was cooled to 0 °C. DCC (16 mg, 0.08 mmol) was added and the reaction mixture was stirred for 20 min at 0 °C and 3 h at 20 °C. Precipitated urea was filtered off and the filtrate was evaporated in vacuo. The residue was dissolved in DCM and, if necessary, filtered again to remove any additional precipitated urea. The DCM solution was washed twice with 0.5 M HCl, once with saturated $NaHCO_3$ solution, and dried over anhydrous $MgSO_4$. After filtration, the solvent was removed in vacuo and the ester **2** was purified by silica gel flash chromatography (Biotage, 25 g column) using 10 CV of DCM to remove DMF and then gradient of MeOH in DCM, 0–15%, 25 CV to obtain final product **2** in 27% yield. ESI-MS calcd for $C_{54}H_{90}N_2O_4$ $[M+H]^+$ 831.69; found 831.73 $[M-H]^-$ 829.8. ^{1}H NMR ([D]$CDCl_3$): $\delta=0.87$ (t, 3H), 1.24 (m, 52H), 1.54 (m, 6H), 1.77 (q, 2H), 2.02 (q, 2H), 2.41 (t, 2H), 3.41 (t, 4H), 3.4–3.47 (m, 4H), 3.55 (t, 2H), 3.62 (m, 1H), 4.01 (t, 2H), 4.12 (dd 1H), 4.22–4.26 (dd, 1H), 7.21 (t, 2H), 7.46 (t, 2H), 7.96 (d, 2H), 8.15 ppm (d, 2H); ^{13}C NMR: $\delta=14.10$, 22.67, 24.44, 26.01, 26.36. 29.68, 31.89, 33.86, 44.86, 54.67, 63.98, 70.19, 70.63, 71.77, 76.45, 122.85, 124.3, 129.7, 132.3, 173.2 ppm.

Equilibrium binding titration by UV/Vis spectroscopy

To quantify binding affinity of EG-Acr (**1**) and L-Acr (**2**) toward dsDNA, absorbance titration at different DNA concentrations was performed keeping the concentration of the ligand constant. The dsDNA used in these experiments was a 4761 bp bacterial plasmid prepared as previously described.[23] Concentration of dsDNA stock solution (8 mM, base-pair concentration) was determined by UV/Vis measurements in TE buffer (20 mM Tris, 2 mM EDTA, 12.5 $MgCl_2$ pH 7.6) using an online oligonucleotide calculator (http://www.basic.northwestern.edu/biotools/oligocalc.html#helpMW). Spectrophotometric titrations of ligands **1** and **2** with dsDNA plasmid were performed at 25 °C by adding increasing amounts (1–5 μL) of dsDNA solution [base pair concentration of 8 mM] to a freshly prepared ligand solution (either 50 μM of **1** dissolved in 1×TEMg (TE buffer supplemented with 12.5 mM $MgCl_2$) or 50 μM of **2** in DMSO. After addition of dsDNA, the mixture was allowed to equilibrate for 5 min before measurements were made. Representative spectra are shown in Figure 1A. Affinity constants were determined from changes in absorbance, according to the equation derived from

© 2015 Wiley-VCH Verlag GmbH & Co. KGaA, Weinheim

neighbor-exclusion models, as previously reported by McGhee and von Hippel (see below).[19,21]

$$\frac{[DNA]}{\Delta\varepsilon_{app}} = \frac{1}{\Delta\varepsilon}[DNA] + \frac{1}{\Delta\varepsilon K_b}$$

$$\Delta\varepsilon_{app} = |\varepsilon_a - \varepsilon_f|, \Delta\varepsilon_{app} = |\varepsilon_b - \varepsilon_f|$$

The intrinsic binding constant, K_b, was calculated from a half-reciprocal plot of the changes in the apparent extinction coefficient, ε_a of ligands versus DNA concentration. The ε_a was calculated from A_{obs}/ligand where A_{obs} was the observed absorbance; ε_f and ε_b correspond to the extinction coefficient for the free and fully bound ligand, respectively. Thermodynamic dissociation constants, K_d, were then calculated as the ratio of the intercept to slope.

Continuous variation binding analysis (Job plot) by fluorescence spectroscopy

To determine dsDNA–ligand binding stoichiometries, the method of continuous variation was carried out similar as described in the literature.[32] Equimolar stock solutions of dsDNA [50 μM base-pair concentration] and acridine ligands [50 μM] were prepared separately in 1×TE buffer. Then 13 samples were prepared where different volumes of both dsDNA and ligand stock solution were mixed to give a final volume of 200 μL. The total molar concentration of the two binding partners (e.g., a dsDNA and ligand) was held constant [50 μM], but their mole fractions were varied. To achieve ligand mole fractions (%L) in a range of 0.05–1, the volume of L was varied from 10–200 μL and the volume of dsDNA was varied from 190–0 μL before mixing. Samples were allowed to equilibrate at RT for 2–3 h before spectroscopic measurements were made. To this end, each solution was filled in a cuvette and fluorescence intensity of the ligands was measured at $\lambda_{Ex/Em}$ = 385/418 nm (*F*1 values). Control samples containing ligand only and buffer in the absence of dsDNA were measured to correct for dilution effects (*F*2 values). Differences in fluorescence ($\Delta F = F2 - F1$) were plotted against the mole fraction of acridine ligand, χ(L).

Assembly of DNA origami

Preparation of ssDNA scaffold strand was carried out as previously described.[23] In brief, dsDNA plasmid 109Z5 (5438 bp) was transformed into ssDNA by nicking with Nb.BbvCI and subsequent digestion with T7 exonuclease. DNA origami was then assembled from solutions containing the 109Z5 ssDNA scaffold strand [700–1200 nM, in 1×TE, pH 8.2] and each of the staple strands [100 μM, in water] in 1×TEMg in a total volume of 0.5–1 mL. The sequence of the 109Z5 ssDNA scaffold strand and the full list of staple strands are given in Tables S1 and S2 in the Supporting Information, respectively. The assembly of origami structures bearing streptavidin molecules (right image in Figure 2C) was achieved by exchanging six staples against biotinylated derivatives (Table S3 in the Supporting Information). Origami structures used for cell uptake studies were modified with nine Cy5-labeled staples (Table S4 in the Supporting Information) and control origami structures bearing covalently attached cholesterol ligands were assembled by using ten cholesterol-labeled staples (Table S5 in the Supporting Information). The annealing was performed by decreasing the temperature from 75 to 25 °C at −6 °C min^{-1} on a PCR cycler (Mastercycler Pro, Eppendorf). After assembly, DNA origami structures were purified from excess staple strands using Amicon ultra-0.5 centrifugal filter units (MWCO 100 kDa, Milipore). Prior to use, the centrifugal filter was washed once with 500 μL of 1×TEMg at 2200 *g* to equilibrate the membrane. The DNA origami solution was concentrated by stepwise addition of 100 μL of origami solution with addition of 600 μL of 1×TEMg buffer and centrifuged for 5 min at 2200 *g* at 4 °C. The concentrated solution was eventually washed five times with 600 μL of 1×TEMg. Subsequently, the solution was collected by centrifugation for 1 min at 1000 *g* to yield 100–200 μL of DNA origami solution. Quality control was performed with AFM and agarose gel analysis using a 1.5% agarose gel in 1×TBEMg buffer (40 mM Tris, 20 mM boric acid, 2 mM EDTA, 12.5 mM Mg acetate, pH 8.00; electrophoresis conditions: 80 V for 2 h at 4 °C). Final DNA origami concentrations were quantified by qPCR and the origami structures were characterized by AFM, as detailed in the Supporting Information. For loading DNA origami structures with acridine ligands, the latter were dissolved in DMSO to a final concentration of 1 mM. Typically, 15 μL [~59 nM] or 25 μL [~68 nM] of DNA origami solution was incubated with 1.6 or 5 μL of ligand to prepare samples of ligand per bp ratio of 0.2 for HeLa cells and ligand per bp of 1 for L929 cells. Samples were incubated with DNA origami solution for 3–4 h. Subsequently, ligand-loaded DNA origami solutions were added to the HeLa or L929 cell cultures in a final concentration of approximately 3.5 and 2.5 nM, respectively, and incubated at 37 °C and 5% CO_2, overnight or 6 h, respectively. After incubation, cells were washed with PBS (+/+) buffer and stained for further investigation using confocal laser scanning microscopy (CLSM). All samples were prepared at least in duplicate.

Cell culture and microscopy

For cultivation of L929 fibroblasts and HeLa cells, 1 mL of an appropriate DMSO stock solution was thawed at 37 °C for 1–2 min and added to a tenfold volume of pre-warmed complete nutrient growth medium containing 10% (v/v) FCS in a culture flask. After 5–6 h incubation in 5% CO_2 atmosphere at 37 °C, the medium was changed with 10 mL of complete nutrient growth medium (supplemented with 10% (v/v) FCS). After incubation, overnight, growth medium (w/o FCS) was exchanged and cells were grown and split after they reached 85–95% confluence. Before subculture, the cell monolayer was washed with PBS (−/−) (Dulbecco's Phosphate Buffer Saline, without calcium and magnesium, Life Technologies, Germany) using approximately half the volume of culture medium. Prior to incubation with DNA origami, cells were seeded in μ-slides (chambered coverslip), eight wells (ibiTreat, tissue culture treated, ibidi, Germany), at a cell density of 3×10^4 cells mL^{-1} for L929 cells and 1×10^4 cells mL^{-1} for HeLa cells and pre-cultured in cell culture medium for 6 h for HeLa cells and 48 h for L929 cells. Quantum 101 (PAA) + 1% penicillin/streptomycin was used as growth medium for HeLa cells and DMEM (Invitrogen) + 1% penicillin/streptomycin + 10% FCS for L929 cells. Cells were stained with Hoechst 33342 for dual color detection of DNA uptake. To this end, cells seeded in eight-well μ-slides were washed with 400 μL PBS (+/+) (Dulbecco's Phosphate Buffer Saline, with calcium and magnesium, Life Technologies, Germany). Medium (400 μL) was added to the cells followed by 100 μL Hoechst 33342 solution (10 mg mL^{-1} in DMSO, Invitrogen, Germany, diluted 1:1000). The cells were incubated for 15 min at 37 °C and 5% CO_2, washed with PBS (+/+) for 5 min and left in PBS (+/+) for CLSM imaging. In some cases, cells were stained with Mitotracker Green (Life Technologies, Germany) for co-localization studies prior to Hoechst 33342 staining. Before staining, cells were washed with 400 μL PBS (+/+). Then 200 μL media was added followed by 1 μL [50 μg mL^{-1}, DMSO] Mitotracker Green (Invitrogen, Germany). Cells were incubated for 30 min at 37 °C and 5% CO_2 and washed (3×)

© 2015 Wiley-VCH Verlag GmbH & Co. KGaA, Weinheim

with PBS (+/+). Images were acquired using an inverted confocal microscope (LEICA confocal fluorescence microscope, TCS SP5, Leica, Germany), equipped with Software Leica Application Suite 2.0.2 (LAS-AF), pinhole: 1 Airy (111.5 μm), resolution: 8 bit and 20× or 60× water objective. Cy5-labeled DNA origami, Mitotracker Green and Hoechst 33342 fluorescence images were acquired by scanning in sequential mode, to avoid cross excitation. Laser intensities did not overcome 30–40%. Confocal *z*-series images were obtained with a 63× water objective. Cy5 excitation was achieved with a HeNe633 (633 nm) laser source and Hoechst 33342 excitation was achieved with an external UV (351 nm) laser source. Mitotracker Green excitation was achieved with an Argon (488 nm) laser source. Images were processed with Leica Application suite, v 2.3.5 imaging software. To quantify the signal intensity of Cy5-labeled DNA origami, the mean fluorescence intensity (MFI) of a scanned area of 20 μm (approximately the size of one attached cell) was measured in two independent experiments (20 cells per experiment). Statistical analysis was performed using GraphPad Prism 6 software. To analyze the viability of HeLa cells, live/dead staining was performed. To this end, 1×10^4 cells were seeded in eight-well μ-slides and propidium iodide (Life technologies, Germany) was used to stain dead cells while CalceinAm (Life technologies, Germany) stained the viable cells. Specifically, cells were washed 1× with PBS (+/+) after sub-culturing. Calcein-AM [10 μM] and propidium iodide [1 μM] solutions were prepared in fresh medium. Cells were incubated in 400 μL of these solutions for 30 min at 37 °C, 5% CO_2 and washed afterwards 3×1 min with PBS (+/+). Fresh medium was then added and cells were analyzed by inverted fluorescence microscopy, equipped with AxioVision software version 4.7 (Axio Imager, Zeiss, Germany).

Acknowledgements

This work was supported by Deutsche Forschungsgemeinschaft (NI 399/10). We thank Barbara Sacca for help with the DNA origami design.

Keywords: DNA nanostructures · intercalators · nucleic acids · self-assembly · surface binding

[1] P. W. Rothemund, *Nature* **2006**, *440*, 297.
[2] J. Nangreave, D. Han, Y. Liu, H. Yan, *Curr. Opin. Chem. Biol.* **2010**, *14*, 608.
[3] W. M. Shih, C. Lin, *Curr. Opin. Struct. Biol.* **2010**, *20*, 276.
[4] B. Saccà, C. M. Niemeyer, *Angew. Chem. Int. Ed.* **2012**, *51*, 58–66; *Angew. Chem.* **2012**, *124*, 60–69; .
[5] A. M. Hung, H. Noh, J. N. Cha, *Nanoscale* **2010**, *2*, 2530.
[6] T. Tørring, N. V. Voigt, J. Nangreave, H. Yan, K. V. Gothelf, *Chem. Soc. Rev.* **2011**, *40*, 5636.
[7] F. C. Simmel, *Curr. Opin. Biotechnol.* **2012**, *23*, 516.
[8] A. Rajendran, M. Endo, H. Sugiyama, *Angew. Chem. Int. Ed.* **2012**, *51*, 874–890; *Angew. Chem.* **2012**, *124*, 898–915; .
[9] Q. Liu, C. Song, Z. G. Wang, N. Li, B. Ding, *Methods* **2014**, *67*, 205.
[10] L. S. Lerman, *J. Mol. Biol.* **1961**, *3*, 18.
[11] A. D. Richards, A. Rodger, *Chem. Soc. Rev.* **2007**, *36*, 471.
[12] B. A. Neto, A. A. Lapis, *Molecules* **2009**, *14*, 1725.
[13] K. Gunther, M. Mertig, R. Seidel, *Nucleic Acids Res.* **2010**, *38*, 6526.
[14] L. Alonso-Sarduy, G. Longo, G. Dietler, S. Kasas, *Nano Lett.* **2013**, *13*, 5679.
[15] H. Özhalici-Ünal, B. A. Armitage, *ACS Nano* **2009**, *3*, 425.
[16] Q. Jiang, C. Song, J. Nangreave, X. Liu, L. Lin, D. Qiu, Z. G. Wang, G. Zou, X. Liang, H. Yan, B. Ding, *J. Am. Chem. Soc.* **2012**, *134*, 13396.
[17] Y. X. Zhao, A. Shaw, X. Zeng, E. Benson, A. M. Nystrom, B. Hogberg, *ACS Nano* **2012**, *6*, 8684.
[18] Y. Ke, G. Bellot, N. V. Voigt, E. Fradkov, W. M. Shih, *Chem. Sci.* **2012**, *3*, 2587.
[19] J. D. McGhee, P. H. von Hippel, *J. Mol. Biol.* **1974**, *86*, 469.
[20] A. D. Papaphilis, Y. H. Shaw, *Biochim. Biophys. Acta* **1977**, *476*, 122.
[21] L. Z. Zhang, G. Q. Tang, *J. Photochem. Photobiol. B* **2004**, *74*, 119.
[22] H. Ihmels, D. Otto, *Top. Curr. Chem.* **2005**, *258*, 161.
[23] M. Erkelenz, D. M. Bauer, R. Meyer, C. Gatsogiannis, S. Raunser, B. Sacca, C. M. Niemeyer, *Small* **2014**, *10*, 73.
[24] F. Moreno-Herrero, J. Colchero, A. M. Baro, *Ultramicroscopy* **2003**, *96*, 167.
[25] S. De Feyter, F. C. De Schryver, *J. Phys. Chem. B* **2005**, *109*, 4290.
[26] Q. Mei, X. Wei, F. Su, Y. Liu, C. Youngbull, R. Johnson, S. Lindsay, H. Yan, D. Meldrum, *Nano Lett.* **2011**, *11*, 1477.
[27] J. Hahn, S. F. Wickham, W. M. Shih, S. D. Perrault, *ACS Nano* **2014**, *8*, 8765.
[28] S. Svedhem, C. A. Hollander, J. Shi, P. Konradsson, B. Liedberg, S. C. Svensson, *J. Org. Chem.* **2001**, *66*, 4494.
[29] M. Botta, S. Quici, G. Pozzi, G. Marzanni, R. Pagliarin, S. Barra, S. Geninatti Crich, *Org. Biomol. Chem.* **2004**, *2*, 570.
[30] K. Fukui, M. Morimoto, H. Segawa, K. Tanaka, T. Shimidzu, *Bioconjugate Chem.* **1996**, *7*, 349.
[31] B. Neises, W. Steglich, *Angew. Chem. Int. Ed. Engl.* **1978**, *17*, 522; *Angew. Chem.* **1978**, *90*, 556.
[32] T. C. Jenkins, in *Drug–DNA Interaction Protocols* (Ed.: K. R. Fox), Humana, Totowa, **1997**, p. 195.

Received: January 8, 2015
Published online on May 14, 2015

© 2015 Wiley-VCH Verlag GmbH & Co. KGaA, Weinheim